Peer-reviewed version available at *Materials* **2019**, *12*, 3656; doi:10.3390/ma12223656

Article

Analysis of the versatility of multi-linear softening functions applied to the simulation of the fracture behaviour of fibre reinforced cementitious materials

A. Enfedaque[1], M. G. Alberti[2], J.C. Gálvez[3,*]

[1] *Departamento de Ingeniería Civil: Construcción, E.T.S de Ingenieros de Caminos, Canales y Puertos, Universidad Politécnica de Madrid. C / Profesor Aranguren, s/n, 28040, Madrid.*; alejandro.enfedaque@upm.es
[2] *Departamento de Ingeniería Civil: Construcción, E.T.S de Ingenieros de Caminos, Canales y Puertos, Universidad Politécnica de Madrid. C / Profesor Aranguren, s/n, 28040, Madrid.*; marcos.garcia@upm.es
[3] *Departamento de Ingeniería Civil: Construcción, E.T.S de Ingenieros de Caminos, Canales y Puertos, Universidad Politécnica de Madrid. C / Profesor Aranguren, s/n, 28040, Madrid.*; jaime.galve@upm.es
* Correspondence: jaime.galve@upm.es; Tel.: +34-910674125

Abstract: Fibre reinforced cementitious materials (FRC) have become an attractive alternative for structural applications. Among such FRC, steel and polyolefin fibre reinforced concrete and glass fibre reinforced concrete are the most used ones. However, in order to exploit the properties of such materials structural designers need constitutive relations that reproduce FRC fracture behaviour accurately. This contribution analyses the suitability of multilinear softening functions combined with a cohesive crack approach for reproducing the fracture behaviour of the FRC previously mentioned. The implementation performed accurately simulates the fracture behaviour while being versatile, robust and efficient from a numerical point of view.

Keywords: cohesive fracture of fibre reinforced concrete, softening functions, fracture behaviour, glass fibre reinforced concrete, polyolefin fibre, steel fibres.

1. Introduction

All cementitious materials are based on having cement as their main binding constituent being also responsible of providing some of the most relevant properties such as their compressive strength and modulus of elasticity. These two properties are highly recommended for construction applications, but some other properties conferred by the cementitious matrix are not as beneficial as the two previous ones. For instance, the flexural strength and the tensile strength of the cementitious materials are limited and consequently might be enhanced if possible. This situation appears in concrete which boasts a remarkable compressive strength and a tensile strength that as a rule of the thumb can be estimated in a tenth of such value. Thus, when constructing structural elements that are subjected to bending moments the stresses that appear would crack the material and even fracture it if the tensile strength is surpassed. Obviously, such event would cause an economic impact on society and might also create a situation where physical damage on humans is inflicted. The traditional solution to such situations has been the use of steel bars placed inside the concrete element section forming reinforced concrete. This approach has been used in a wide variety of applications both in civil engineering and architecture. However, in the nineteenth century the possibility of creating a continuous reinforcement in concrete by adding fibres appeared. From that moment onwards the use of fibres became an option to be considered based on the positive effect of the randomly distributed fibres in the mechanical properties of concrete.

If fibres are distributed during concrete mixing their distribution can be considered random and the material manufactured is usually termed as fibre-reinforced concrete (FRC). Conventionally, steel fibres have been the most used ones in concrete structural elements and accordingly the material created has been described as steel fibre reinforced concrete (SFRC). The usage of such fibres has been

Peer-reviewed version available at Materials 2019, 12, 3656; doi:10.3390/ma12223656

extensive and enormously successful as the steel fibres provide not only increments in tensile and flexural strength alike but also in shear strength [1]. Moreover, the ductility of the material is greatly enhanced. There are applications of steel fibres such as industrial pavements and airport runways, shotcrete, and precast elements as well as other uses [2]. These examples have been performed based on the results of experimental campaigns that assessed the tensile behaviour, the fatigue performance or the impact response of SFRC [3, 4]. As was shown in such papers steel fibres confer plain concrete remarkable mechanical properties especially at low strains. Nonetheless, the durability of the concrete elements might be, in certain environments, compromised as steel fibres are corrodible.

Macro-polymer fibres with structural capacity have appeared recently as a possible addition to concrete. Such fibres do not suffer corrosion due to their plastic nature even when concrete is placed in chemically harmful environments. Moreover, this type of fibres might reduce the economic impact on concrete of the increment of the steel prices. Recent research has shown that polyolefin fibre reinforced concrete (PFRC) fulfils the requests established in the recommendations [5, 6, 7, 8] and therefore their contribution to the properties of the concrete element might be considered in the structural design [9].

While it is true that most of the applications of fibres in civil engineering and architecture imply their use in structural elements, it should not be overlooked that some cementitious materials with non-structural uses are also widespread. This is the case of GRC, which is formed by cement mortar and chopped glass fibres. GRC has been employed in reduced-thickness building elements in which shrinkage may cause cracks. The presence of glass fibres randomly distributed avoid this phenomenon. Furthermore, they do not only enhance the flexural and tensile strength, but also provide ductility to a certain extent. The use of GRC has ranged from permanent concrete moulds, communication structures, and façade panels to gutters [10]. Such uses of GRC might imply lowering the cost of the structure and while obtaining a nice final appearance of the structures. Such aspects would be useless if notable mechanical properties of GRC were not achieved.

The structural design and numerical codes consider the fracture behaviour of the fibre-reinforced cementitious materials in order to fully exploit the improvements in the mechanical properties and ductility. In order to reproduce the appearance of cracks and their development in the cementitious matrices, several numerical approaches have been applied. Some models have considered that the focus should be on the overall cracking process without dealing with the single cracks. One of such approaches was termed the smeared crack approach [11]. These implementations were notoriously successful in the cases where there were no localised cracks and a limited crack opening was detected. Some others have been applied if a detailed study of the appearance and development of cracks was required. Recently, one of these approaches was based on enriching the amount of degrees of freedom of the nodes that compose the finite element. Such method, which was termed extended finite element method (XFEM), consumed a great amount of computer power although it was able to obtain promising results. Such approach was not only used to model the bond between carbon fibre reinforced polymers (CFRP) and concrete but also to reproduce the compressive behaviour of rubberised concrete or the behaviour of concrete reinforced with steel fibres [12, 13, 14, 15]. Unfortunately, the promising results of XFEM were not transferable to all situations and in some other approaches were not applicable. The cohesive crack model was developed by Hillerborg in the early 1970's [16] and was firstly applied to plain concrete. Afterwards, the model was modified in order to consider certain material variations such as those that might appear in other quasi-brittle materials such as brick masonry [17, 18, 19]. Besides, the cohesive crack model was able to reproduce the failure of plain concrete under a combination of bending and shear stresses, which is commonly known as mixed mode due to the combination of modes I and II. One of the main contributions of this model is the absence of a tracking algorithm which pre-determines the location of the cracks [20].

The cohesive crack model has based its success in various factors. Among them, the direct applicability of the laboratory mechanical properties test into such model suppose a significant advantage. When applied to plain concrete the model parameters required are: tensile strength, modulus of elasticity and fracture energy. Such values can be obtained in laboratory by means of standard codes or using several recommendations [21, 22, 23, 24]. Once such parameters have been found, the fracture behaviour of the material requires a certain softening function to be proposed.

Peer-reviewed version available at Materials 2019, 12, 3656; doi:10.3390/ma12223656

Although several authors have analysed the applicability of exponential functions to plain concrete with successful results, the use of linear, bi-linear or multi-linear functions cannot be overlooked. The latter functions have been profusely used due to their simplicity and the accurate simulations of the material behaviour obtained.

This contribution analyses the changes that should be carried out when choosing the type of multi-linear softening function in order to reproduce with accuracy the fracture behaviour of several types of FRC. The numerical simulations are compared with the experimental results. In addition, the changes needed to capture the influence of the fibre dosage, the type of fibres and the variations of the matrix properties are analysed. Consequently, the experimental results obtained with specimens coming from several formulations of PFRC, GRC and SFRC are simulated. Finally, all softening functions are examined and trends and differences outlined.

2. Description of the model

The cracking process in fibre reinforced cementitious materials is a matter that has focused several studies in the last decades. Using different techniques the behaviour of such materials has been simulated using for instance zero thickness elements or employing inverse analysis [25, 26]. By applying such techniques, the fracture behaviour of ultra-high strength fibre reinforced concrete has been simulated [27, 28]. Moreover, if the cohesive crack approach is used both the PFRC and GRC fracture behaviour have been reproduced successfully [6, 29]. The embedded cohesive crack model implemented is based on a central forces model that is explained below.

The fracture behaviour of the material is introduced by using two parameters. The first one is the fracture energy, obtained by means of laboratory tests. The second one is the shape of the softening function. It has to be underlined that several softening functions can be proposed while maintaining the same amount of fracture energy. However, boasting the same fracture energy does not necessarily imply obtaining an accurate fracture behaviour reproduction. Consequently, to reproduce the fracture behaviour is not only needed the amount of fracture energy, but also finding the appropriate shape of the softening function. Therefore, the shape of the softening function might be considered a property of the FRC which could be influenced by the geometric and mechanical properties of the fibres and the characteristics of the fibre-matrix interface among other factors [30].

The softening function defines the behaviour of the material when the tensile strength is surpassed. The initial instant corresponds to a null crack width, and inability of the material to sustain any stress determines the critical crack opening. The fracture energy is determined by integrating the area below the stress-crack width curve from a null crack width to the critical crack width, w_c. At this crack width the stress becomes zero. At any other crack opening w the value of the tensile stress is determined by $f(w)$ as it is shown in Equation (1).

$$G_F = \int_0^{w_c} f(w)dw \quad (1)$$

If the maximum stress reaches the tensile strength (f_{ct}) the fracture behaviour starts and equation (2) is confirmed.

$$f_{ct} = f(0) \quad (2)$$

The first uses of the cohesive crack models implemented linear, bilinear or even exponential softening functions in order to capture the cracking process of plain concrete [31]. One of such possibilities can be seen in equation (3).

$$\sigma = f_{ct}.e^{\left(-\frac{f_t \omega}{G_F}\right)} \quad (3)$$

where f_{ct} is the tensile strength and G_F stands for the specific fracture energy. Using such function accurate results were found for plain concrete. Figure 1 shows a sketch of the softening function for mode I fracture of plain concrete.

Preprints (www.preprints.org) | NOT PEER-REVIEWED | Posted: 4 October 2019 doi:10.20944/preprints201910.0050.v1

Peer-reviewed version available at Materials 2019, 12, 3656; doi:10.3390/ma12223656

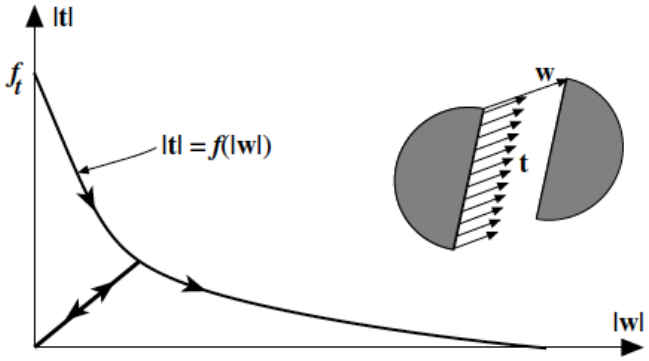

Figure 1. Sketch of the softening curve, with unloading branch, and central force model for the cohesive crack model.

However, the shapes of the softening functions proposed for plain concrete are not apt for FRC. In order to minimise the expense of checking the suitability of various possibilities, the concept of inverse analysis was adopted. Inverse analysis is based on adjusting the numerical response of the model to the experimental behaviour by a trial-and-error optimisation implemented in a finite element code [32, 33]. As the bilinear softening function merged both accuracy of the simulation and a low computational expense, the beneficial presence of fibres was simulated by adding linear stretches to the softening function. Consequently, the bilinear softening function was transformed into a tri-linear one and the latter into a multi-linear one if more stretches were added.

The model used in this study is based on the embedded cohesive crack model [17, 18] that enables the numerical simulation of concrete fracture and is extended to FRC. It entails the assumption of the crack displacement vector **w** be parallel to the traction vector **t** and with a continuously increasing opening of the crack $|\mathbf{w}|$ the relation can be seen in equation (4).

$$\mathbf{t} = \frac{f(|\mathbf{w}|)}{|\mathbf{w}|}\mathbf{w} \quad (4)$$

In order to consider unloading processes, the cohesive crack unloads to the origin and (4) becomes equation (5), (see Figure 1).

$$\mathbf{t} = \frac{f(|\tilde{\mathbf{w}}|)}{|\tilde{\mathbf{w}}|}\mathbf{w} \qquad \text{being } \tilde{\mathbf{w}} = max(|\mathbf{w}|) \quad (5)$$

being $\tilde{\mathbf{w}}$ the historical maximum magnitude of **w**.

The constitutive relations were implemented in a material subroutine within a FEM code. The material behaviour was introduced in the program by means of a constitutive relation with different behaviour under tensile and compressive stresses. Under compressive stresses the material behaved as linear elastic being its module of elasticity that found in the laboratory tests. In addition, no damage under compressive stresses was considered. In the case of tensile stresses, before reaching the tensile strength of the material the behaviour was linear elastic being the stress-strain relation governed by the modulus of elasticity. However, once the tensile strength was reached the behaviour of the material followed the softening function proposed. In the event of unloading the material moved towards the origin, the zero-strain and zero-stress situation, in a linear manner. If a reloading process occurred, the material was loaded following the same slope defined in the unloading process until reaching the maximum crack width previously suffered by the material. If the crack continued growing the remaining of the softening function was followed. These characteristics were common to all the proposals of softening functions tested.

Figure 2a shows a random classical finite element determined by a node arrangement. A straight crack is assumed to be embedded in it. As Figure 2b shows, the crack divides the element in the two sub-domains A^+ and A^-. One of the sides of the crack is taken as the reference, in this case the corresponding with the sub-domain A^-, with its normal **n** pointing towards the other side and considering it as the positive normal. If **w** is defined as the displacement jump across the crack of the opposite side of the crack with respect to the reference side (see Figure 2b). Following the strong

Preprints (www.preprints.org) | NOT PEER-REVIEWED | Posted: 4 October 2019 doi:10.20944/preprints201910.0050.v1

Peer-reviewed version available at Materials 2019, 12, 3656; doi:10.3390/ma12223656

discontinuity approach (SDA), the approximate displacement field within the element can be expressed as follows:

$$\mathbf{u}(\mathbf{x}) = \sum_{a \in A} N_a(\mathbf{x})\mathbf{u}_a + [H(\mathbf{x}) - \boldsymbol{N}^+(\mathbf{x})]\mathbf{w} \qquad (6)$$

where a is the index of the element node, $N_a(\boldsymbol{x})$ is the shape function for node a, $\mathbf{u}_a$ the corresponding nodal displacement, $H(\boldsymbol{x})$ the Heaviside jump function across the crack plane, which represents a unit step placed along the crack line that also can be defined as the integral of the Dirac's δ function on the crack line [i.e., $H(\mathbf{x}) = \mathbf{0}$ for $\mathbf{x} \in \mathbf{A}^-$, $H(\mathbf{x}) = 1$ for $\mathbf{x} \in \mathbf{A}^+$], and

$$\boldsymbol{N}^+(\mathbf{x}) = \sum_{a \in A^+} N_a(\mathbf{x})$$

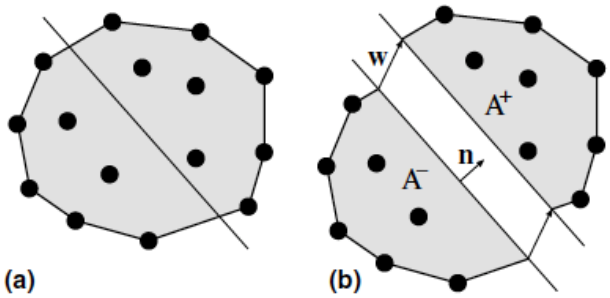

Figure 2. a) Generic element with nodes and crack line, b) displacement jump across the crack line boasting a crack with uniform opening.

From the displacement field the strain tensor can be determined as a continuous part $\boldsymbol{\varepsilon}^c$ plus Dirac's δ function on the crack line. The continuous part, which defines the stress field on the element on both sides of the crack, is obtained by the following:

$$\boldsymbol{\varepsilon}^{\mathbf{c}}(\mathbf{x}) = \boldsymbol{\varepsilon}^a(\mathbf{x}) - [\mathbf{b}^+(\mathbf{x}) \otimes \mathbf{w}]^S \quad (7)$$

where $\boldsymbol{\varepsilon}^a$ and $\mathbf{b}^+$ are given by

$$\boldsymbol{\varepsilon}^a(\mathbf{x}) = \sum_{a \in A} [\mathbf{b}_a(\mathbf{x}) \otimes \mathbf{u}_a]^S \quad (8)$$

$$\mathbf{b}^+ = \sum_{a \in A^+} \mathbf{b}_a(\mathbf{x}) \quad (9)$$

with $\mathbf{b}^+ = \text{grad}\, N_a(\mathbf{x})$. Also the superscript S stands for the symmetric part of a tensor. Also, $\boldsymbol{\varepsilon}^a$ is the apparent strain tensor of the element which was obtained from the nodal displacements.

As it has been said before, an assumption regarding the bulk material, which is not affected by the cracking process, has been made in order to simplify the computations. Such assumption is that the material outside the crack behaves as isotropic having a linear-elastic response. The crack displacement vector $\mathbf{w}$ is obtained at the level of the crack in the constant strain triangle finite element used considering it as two internal degrees of freedom.

The implementation follows an algorithm similar to plasticity in order to calculate the stress tensor in the element. If the elasticity of the bulk material is adopted as was previously mentioned the stress tensor can be provided by equation (10). Thus, the stress tensor is expressed as follows:

$$\boldsymbol{\sigma} = \mathbf{E}: [\varepsilon^a - (\mathbf{b}^+ \otimes \mathbf{w})^S] \quad (10)$$

Preprints (www.preprints.org) | NOT PEER-REVIEWED | Posted: 4 October 2019 doi:10.20944/preprints201910.0050.v1

Peer-reviewed version available at Materials 2019, 12, 3656; doi:10.3390/ma12223656

In Equation (10) $\mathbf{E}$ stands for the tensor of elastic moduli. However, the displacement of the crack should be obtained before calculating the result of the stress. The jump vector $\mathbf{w}$ and the traction vector $\mathbf{t}$ are related by Equation (4) along the cohesive crack. The traction vector is computed locally for obtaining the exact solution, as:

$$\bar{\mathbf{t}} = \boldsymbol{\sigma}\,\mathbf{n} \quad (11)$$

For the finite element, however, the approximate tractions and crack jump vectors should be considered. The traction field along the crack line is approximated by a constant traction $\mathbf{t}$ .in order to simplify the solution. The corresponding equation is obtained by substituting the foregoing expression by the stress (10) into Equation (11) and the result into the cohesive crack Equation (2). The resulting condition is as follows:

$$\frac{f(|\widetilde{\mathbf{w}}|)}{|\widetilde{\mathbf{w}}|}\mathbf{w} = [\mathbf{E}\colon \varepsilon^{a}] \cdot \mathbf{n} - [\mathbf{E}\colon (\mathbf{b}^{+} \otimes \mathbf{w})^{S}]\mathbf{n} \quad (12)$$

which can be rewritten as

$$\frac{f(|\widetilde{\mathbf{w}}|)}{|\widetilde{\mathbf{w}}|}\mathbf{w} = [\mathbf{E}\colon \varepsilon^{a}] \cdot \mathbf{n} - [\mathbf{n} \cdot \mathbf{E}\colon \mathbf{b}^{+}]\mathbf{w} \quad (13)$$

or

$$\left[\frac{f(|\widetilde{\mathbf{w}}|)}{|\widetilde{\mathbf{w}}|}\mathbf{1} + [\mathbf{n} \cdot \mathbf{E} \cdot \mathbf{b}^{+}]\right]\mathbf{w} = [\mathbf{E}\colon \varepsilon^{a}] \cdot \mathbf{n} \quad (14)$$

where $\mathbf{1}$ is the second-order unit tensor. This equation is solved for $\mathbf{w}$ **by** using the Newton-Raphson method given the nodal displacements (and so $\boldsymbol{\varepsilon}^{a}$) once the crack is formed with $\mathbf{n}$ and $\mathbf{b}^{+}$ thus also being obtained. Additional details of the model may be found in ref [17, 18, 19].

3. Suitability of the multilinear softening functions

The softening functions applied to simulate the fracture process of FRC were chosen according to the material characteristics. Accurate results were found in literature [19] when bilinear functions were used for simulating the fracture behaviour of plain concrete. However, when fibres were added, several characteristics of the experimental load-deflection curves suggest introducing more complex constitutive relations. When selecting the softening function not only the fibre geometry, but also some other characteristics such as their tensile strength, modulus of elasticity or even the type of anchorage between the fibres and matrix had to be considered. Consequently, in the case of a frictional bond between the fibres, with a moderate stiffness, a three-stretch softening function was selected. This approach was applied when reproducing the fracture behaviour of materials such as GRC or PFRC where the fibres boast a straight shape

In the case of steel fibres some other considerations had to be taken into consideration. Steel fibres are approximately between 2.8 times and 20 times stiffer than glass fibres and polymeric fibres correspondently. Moreover, the type of anchorage depends on the shape of the fibres. Nowadays, steel-fibre manufacturers offer a wide variety of shapes such as straight, sinusoidal, simple-hooked, multiple-hooked or flat among others. Nevertheless, hooked steel fibres are the most employed. Such fibres offer a two-way anchorage when added to concrete. Firstly, there is remarkable chemical compatibility between steel and the hydrated cement compounds which generates a frictional bond between the matrix and the fibres. Secondly, the hooks of the fibres create a mechanical grip between both materials. The importance of the mechanical anchorage is much greater that the chemical one and is responsible for most of the load bearing capacity of the composite material when the width of the cracks is still reduced. The characteristics previously cited were capital for introducing modifications in the softening functions chosen for GRC and PFRC. Therefore, a four-stretch function was chosen. The outlook of the softening functions can be seen in Figure 3

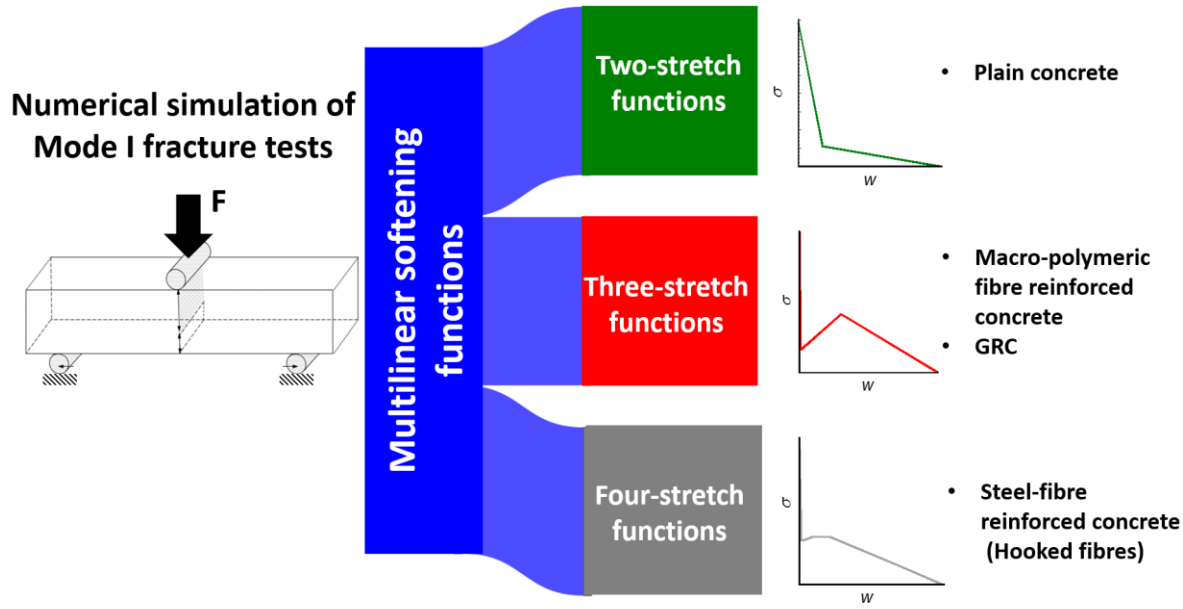

Figure 3. Softening functions selection for distinct types of fibres.

The implementation of the proposed softening function for GRC and PFRC can be seen in equation (15). Nonetheless, the values of the parameters that define the geometry of the softening functions vary remarkably between both materials.

$$\begin{cases} \sigma = f_{ct} + \left(\dfrac{\sigma_k - f_{ct}}{w_k}\right) w & if \quad 0 < w \le w_k \\ \sigma = \sigma_k + \left(\dfrac{\sigma_r - \sigma_k}{w_r - w_k}\right)(w - w_k) & if \quad w_k < w \le w_r \\ \sigma = \sigma_r + \left(\dfrac{-\sigma_r}{w_f - w_r}\right)(w - w_r) & if \quad w_r < w \le w_f \\ \sigma = 0 & if \quad w > w_f \end{cases} \tag{15}$$

In the case of the softening function which corresponds to SFRC the four-stretch function was implemented as can be seen in equation (16)

$$\begin{cases} \sigma = f_{ct} + \left(\dfrac{\sigma_k - f_{ct}}{w_k}\right) w & if \quad 0 < w \le w_k \\ \sigma = \sigma_k + \left(\dfrac{\sigma_r - \sigma_k}{w_r - w_k}\right)(w - w_k) & if \quad w_k < w \le w_r \\ \sigma = \sigma_r & if \quad w_r < w \le w_t \\ \sigma = \sigma_r + \left(\dfrac{-\sigma_r}{w_f - w_t}\right)(w - w_t) & if \quad w_t < w \le w_f \\ \sigma = 0 & if \quad w > w_f \end{cases} \tag{16}$$

At this point, the final stage is to establish the values of the parameters that define the softening functions. In the case of the three-stretch one the values k (w_k, σ_k), r (w_r, σ_r) and f (w_f, 0) had to be defined. Correspondently, in the case of the four-stretch function the values of k (w_k, σ_k), r (w_r, σ_r) , t (w_t, σ_r) and f (w_f, 0) had to be established. It should be highlighted that the generic expression that could offer a four-stretch function has been modified to consider a stretch of constant stress between k and t.

The methodology used in order to determine the aforementioned parameters is commonly known as inverse analysis. The process can be observed applied to one formulation of GRC in Figure 4. In the first stage a proposal of the parameters, k, r and f is made. Such values are implemented in the material subroutine and after the simulation has been carried out the correspondent numerical curve is obtained. At the second stage, the accuracy of the numerical calculation is checked as well as the amount of fracture energy consumed (G_f). If the prediction does not fit either of the cited parameters a new proposal of k, r and f is assumed. This step is

Preprints (www.preprints.org) | NOT PEER-REVIEWED | Posted: 4 October 2019 doi:10.20944/preprints201910.0050.v1

Peer-reviewed version available at Materials 2019, 12, 3656; doi:10.3390/ma12223656

repeated as long as necessary in order to obtain an accurate reproduction of the shape of the experimental curves and the value of the fracture energy.

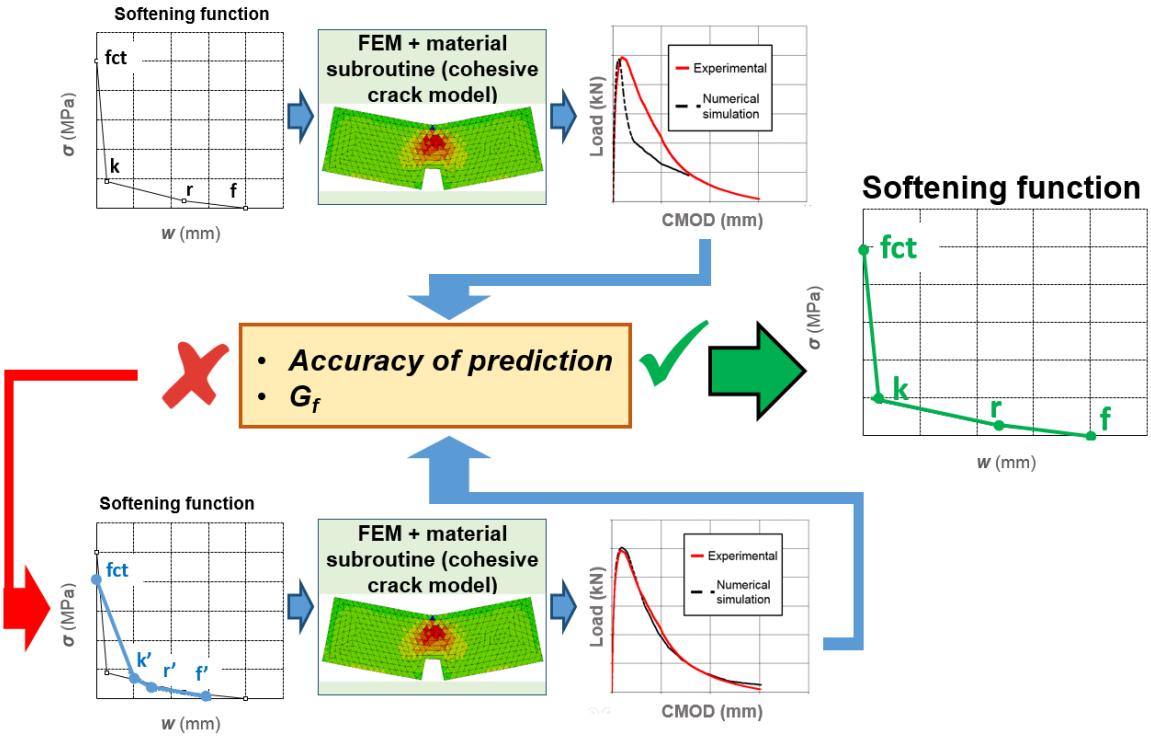

Figure 4: Iterative procedure used to obtain the softening functions

4. Materials and tests

The test specimens for the numerical simulations were produced in previous experimental campaigns. Two types of cementitious matrixes were used: one for steel and polyolefin fibres and a mortar for GRC. In the case of steel and polyolefin macro fibres, a self-compacting concrete was designed. The mix proportioning was previously achieved with the objectives of maintaining self-compactability even after adding the fibres but also with moderate cement and admixture contents. The aggregate distribution was designed by the maximum dry density criterion and the paste design required 375 kg/m³ of cement. In addition Sika Viscocrete-5720 admixture with a 1.25% of cement weight of and 200 kg/m³ of limestone powder addition were used. The mix proportioning can be observed in Table 1. The tests were performed in accordance with RILEM TC-187 SOC [34]. According to the standard, a notch of a third of the height of the sample was performed in the centre of the sample and the relation between span and height in the test was set as 3.0. The loading cylinder was placed in the centre of the sample. For every concrete type, three prismatic specimens of dimensions 430 x 100 x 100 mm³ were cast and tested. The simulations were performed with the average curve of each concrete type.

Table 1. Concrete mix proportioning

Material	SFRC	PFRC3	PFRC4.5	PFRC6	PFRC10
Cement (kg/m³)	375	375	375	375	375
Limestone powder (kg/m³)	200	200	200	200	200
Water (kg/m³)	187.5	187.5	187.5	187.5	187.5
Sand (kg/m³)	918	918	918	918	918
Grit (kg/m³)	245	245	245	245	245
Gravel (kg/m³)	367	367	367	367	367
w/c	0.50	0.50	0.50	0.50	0.50
Steel fibres (kg/m³)	26	-	-	-	-

Polyolefin fibers (kg/m³)	-	3	4.5	6	10
Superplasticizer (kg/m³)	4.7	4.7	4.7	4.7	4.7

.

Regarding GRC, three formulations were used with the mix proportions shown in Table 2. The main differences among them was the use of two admixtures called Powerpozz and Metaver. The former is product of pozzolanic nature whereas Metaver a kaolin thermally treated. The test boards produced were 1200 x 1200 mm² and 10mm thick approximately. These boards were produced by simultaneous projection of cement mortar and chopped 38mm-long glass fibres using the same process that is commonly used in GRC industry. The volumetric fraction of fibres was of 5%. From each type of GRC board, three rectangular 172 x 55 x 10mm³ specimens were obtained. As in the case of concrete TC-187-SOC was intended to be applied in GRC tests. Nevertheless, the magnitudes of the specimens had to be modified as result of the GRC thickness. If the thickness of GRC were increased the reduced weight of GRC would increase losing one of the major advantages of the material. However, the rest of suggestions have been followed as close as possible. Deeper detail of the production and testing can be found in reference [29]. As in the concrete tests and according to the standard, the relation between the span and the height of the sample was set as 3.0 and the depth of the central notch was one third of the height. In the case of the GRC samples the height was 55mm.

Table 1. Concrete mix proportioning

	Cement (kg)	Sand (kg)	Water (kg)	Plasticizer (l)	Addition (kg)
GRC	50	50	17	0.5 litres	----------
GRC with Metaver® (GRC-M)	50	50	23	0.5 litres	12.5
GRC with Powerpozz® (GRC-P)	50	50	25	0.5 litres	12.5

5. Results and discussion

The implementation that has been previously described was employed to simulate several fracture tests. Initially, fracture tests of 100x100x430mm³ specimens of self-compacting PFRC with 3, 4.5, 6 and 10kg/m³ of 60mm-long polyolefin fibres were reproduced. The experimental plots show at least the results obtained in three tests. In Figure 5 it can be seen the results of the simulations. Such curves clearly shows that the tri-linear softening function was able to reproduce the fracture characteristics of PFRC with notable precision. The comparison between the experimental results can be seen in Figure 5 (right). The implementation carried out has shown versatility, robustness and efficiency from a numerical point of view. By changing the points k, r and f that define the softening function it was possible to simulate all the characteristics of the fracture tests such as the variations of the minimum post-cracking load which changed markedly among the PFRC. Likewise, the maximum experimental post-cracking loads were captured in the numerical curves together with the slopes of the after peak loading branch and the after peak unloading branch. As can be seen in Figure 5 the experimental curves were precisely reproduced.

Preprints (www.preprints.org) | NOT PEER-REVIEWED | Posted: 4 October 2019 doi:10.20944/preprints201910.0050.v1

Peer-reviewed version available at Materials 2019, 12, 3656; doi:10.3390/ma12223656

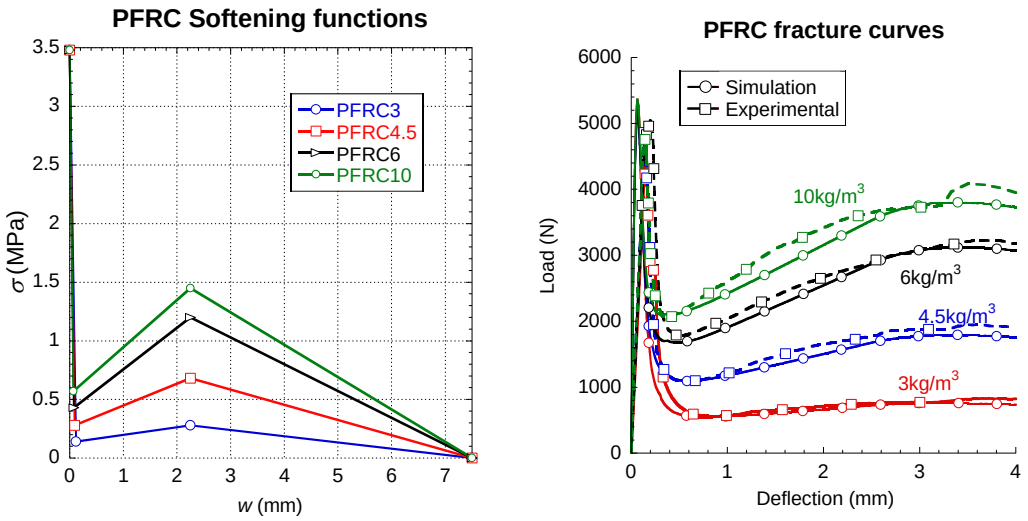

Figure 5: Softening functions (left) and comparison among simulated and experimental results (right).

In order to check the suitability of the tri-linear softening curves when applied to other cementitious material with fibres GRC fracture tests were analysed. Three GRC preparations were simulated in accordance with the experimental results. It should be underlined that among them the only difference was the usage of certain chemical products that intend to inhibit the modification of properties that suffer traditional GRC with aging processes. The traditional formulation was named GRC and the formulation with Powerpozz and Metaver were termed GRC-P and GRC-M respectively. The tests carried with the mixes of GRC could not be carried out as stated in any recommendation, as there was not any standard suitable for that purpose at that time. Likewise to the experimental curves of PFRC, in Figure 6 are plotted at least the average of three valid tests. Such results showed a notably low scatter.

The softening functions implemented in the case of the GRC formulations were tri-linear and consequently were defined by three stretches. This approach is similar to the one taken in the case of PFRC. The modifications that were introduced in the parameters that describe the softening functions were capable of reproducing the fracture tests of GRC with noteworthy precision. Such variation in the parameters were able to adapt the simulated fracture behaviour of GRC to the experimental one and reproduce not only the ductility, and the maximum load sustained but also the unloading process that the materials showed. Based on the softening curves obtained it can be said that there is no apparent relation between the maximum load of the fracture test and the tensile strength of the GRC formulation. Furthermore, the maximum load registered seems to be related with the slope of the first stretch of the softening function. Such assumption can be performed by contrasting the curves of GRC-P and GRC. Although in such curves it can be seen that GRC-P boasts a higher maximum load the tensile strength of both materials is the same. Consequently, it might be the greater slope of the unloading branch the responsible of such different maximum load.

The most important parameter of the softening functions that define the ductility of the material is the critical crack width, w_c. Nevertheless, as can be seen in Figure 6 w_c is not the only factor that should be evaluated. Although GRC-M and GRC boast the same value of w_c the maximum CMOD varies between both formulations. Consequently, the slope of the last part of the softening curves might have an influence that deserves to be considered.

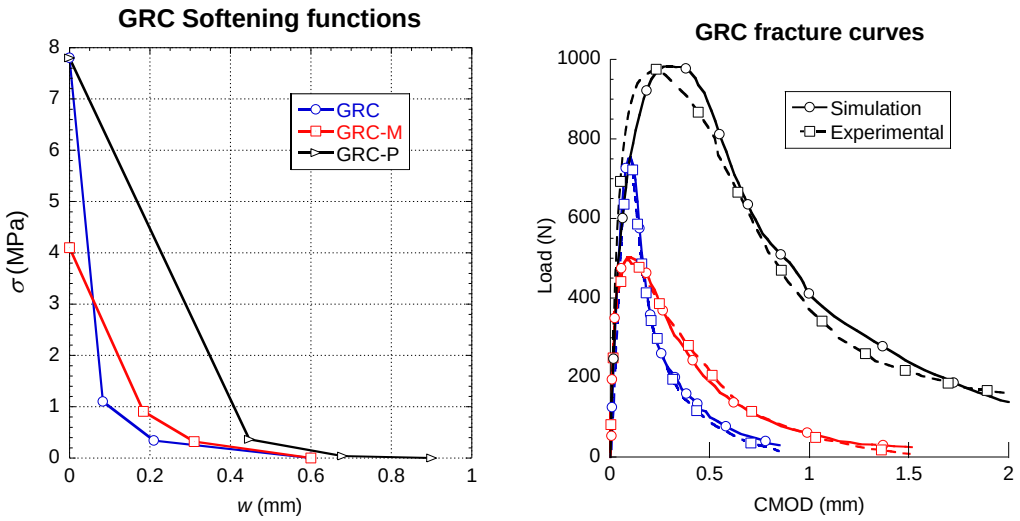

Figure 6: Softening functions (left) and comparison between simulated and experimental results (right).

Lastly, the experimental results obtained in three-point bending fracture tests of a SFRC with a fibre dosage of 26kg/m³ have been simulated. The tests were conducted in 100x100x430mm³ specimens. A similar process to the case of the PFRC specimens was followed both for concrete production and fracture tests. RILEM-TOC 187 was the recommendation followed. The experimental curves shown in Figure 7 are the average of at least three successful tests which also showed scarcely any scatter. In this case the tests were reproduced numerically by using a multilinear softening function (with four stretches). The modification of the tri-linear functions previously cited was based on the outlook of the experimental curve. Such curve boasted approximately between 0.5 and 1.2mm of deflection an area that could be identified as a plateau. Consequently such feature was added to the tri-linear softening function. In addition, such plateau could be the reflection of the area where the hooks prevent the fibre from being extracted. Therefore, in this area the fibres behave as if they were elastically deformed. After this area the deformation of the hooks and the extraction of the fibres begun and consequently the softening curve showed an unloading branch until the load-bearing capacity of the material vanished. The outlook of the softening function employed can be seen in Figure 7. By defining the values of k, r, t and f using the cited inverse analysis an accurate reproduction of the experimental behaviour of the SFRC could be reproduced. It was possible to tune not only the peak load of the test but also other features of great relevance such as the minimum post-peak load, the maximum post-peak load, the shape and load value of the plateau and the unloading process.

Preprints (www.preprints.org) | NOT PEER-REVIEWED | Posted: 4 October 2019 doi:10.20944/preprints201910.0050.v1

Peer-reviewed version available at Materials 2019, 12, 3656; doi:10.3390/ma12223656

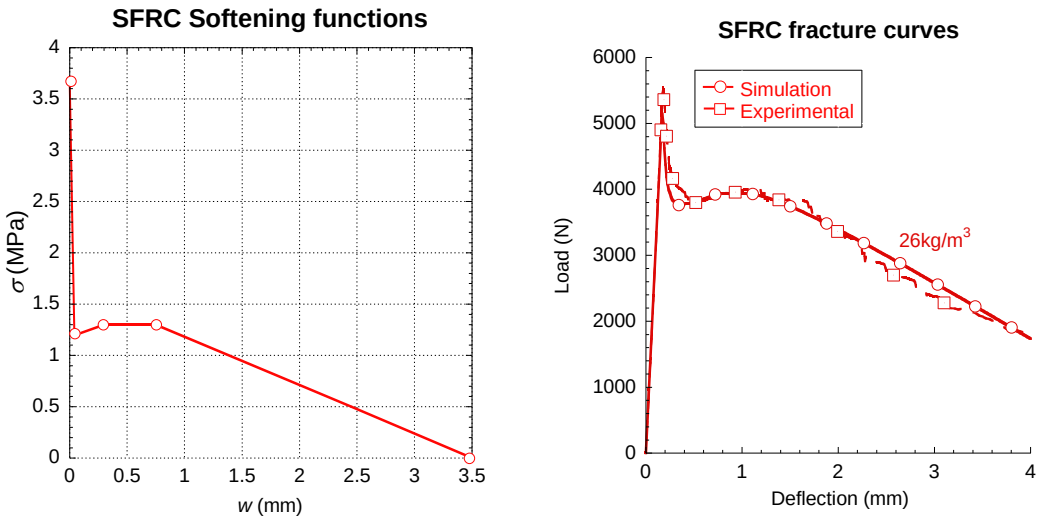

Figure 7: Softening functions (left) and comparison between simulated and experimental results (right).

Comparing the characteristics of the functions implemented it might be said that the maximum load registered in the fracture tests in mainly determined by the tensile strength only if the slope of the first stretch is a relatively large negative value. If such value is greater the maximum load of the fracture test might be influenced by the combination of the tensile strength and the slope. Such comment has been shown valid for several materials, types of fibres or even geometries of the specimens tested. GRC-P maximum load is a clear example of this situation. In the correspondent fracture curves the material is capable of increasing the total load sustained although the tip of the notch is partially damaged. The simulations were able to reproduce the previously commented phenomenon and the elements placed in the whereabouts of the notch tip were damaged before the maximum load was reached.

In order to complete the discussion of the results, Figures 5-7 are compared and analysed in more detail. In the figures, it possible to realise fibre type and shape has strong influence in the constitutive relations of the composite material. Short straight fibres such as glass fibres and with higher elasticity modulus than concrete produce increments of the overall fracture energy and the maximum tensile strength, although a softening behaviour is appreciated in the post-cracking branches. The good tensile properties and the mechanical anchorage of steel hooked fibres limit the first unloading branch and the constitutive relation showed a remarkable horizontal plateau. The polyolefin fibres are macro-fibres with embossed surface and lower elasticity modulus than the other fibres and the concrete matrix. This supposed in the constitutive relation a trilinear post-cracking behaviour with three turning points. The first is the beginning of pronounced descend of strength down to certain opening of the crack (the second turning point) at which the fibres are capable of bearing the stress and a recharging branch appears and it seems that various mechanisms are taking place such as fibre bridging and fibre sliding at the same time. At certain crack opening, the constitutive relation reaches the maximum post-cracking strength and start discharging again. These three main type of behaviour represent most of the mechanisms of fibre reinforced composite materials. Having said that, this study has shown how multilinear softening branches are a powerful tools together with cohesive fracture behaviour in order to build the constitutive relation of this type of composite materials

6. Conclusions

Multilinear softening functions have been successfully implemented in a commercial finite element code employing a material user subroutine. Using these functions, fracture tests of

PFRC, SFRC and GRC were simulated with notable precision. The numerical processes carried out have shown versatility, robustness and efficiency from a numerical point of view.

It is worth noting that this procedure permits achieving constitutive relations that could serve for the structural design of elements with three types of fibre reinforced cementitious materials. That is to say, this procedure and model can be used to find the softening functions of FRC. This study has shown the outstanding possibilities of multi-linear functions and the cohesive crack model in order to achieve accurate results. Moreover, it is important to clarify, that in order to use this model as a predictive model, physical meaning of the turning points must be found and related with other material properties or fibre characteristics or dosages.

The shapes of the fracture curves registered in the tests carried out in GRC and PFRC have been accurately reproduced. This has been possible by modifying the points that determine the characteristics of the softening curves which have been capable of simulate the load regain characteristic of the PFRC curves and the load decrement experimented by the GRC formulations.

The influence of the chemical products added to the GRC formulations and the effect of the dosage of fibres have been analysed by modifying the length and slope of the stretches of the softening curves. Such approach were able to reproduce the typical ductility while unloading of GRC and the steep load decrement followed by a load regain and a gradual unloading characteristic of PRFC.

In the case of having a high slope in the first stretch of the softening curve the maximum load register in the fracture test was mostly influenced by the tensile strength of the cementitious material. Nonetheless, when such slope is less steep the maximum experimental value is influenced by a combination of such slope and the tensile strength. As far as the ductility is concern, it is mainly influenced by w_c.

Lastly, a more complicated anchorage system generates an increment of the number of stretches of the softening functions as detected when comparing the reinforcement of concrete with hooked steel fibres, polyolefin fibres and glass fibres. Subsequently, in the case of steel fibres with more complex geometries an increment of the number of hooks or the use of sinusoidal fibres might result in multi-linear softening functions with more than four stretches.

Acknowledgements

The authors gratefully acknowledge the financial support provided by Ministry of Economy, Industry and Competitiveness of Spain by means of the Research Fund Project BIA2016-78742-C2-2-R.

References

[1] A. Picazo, J. C. Gálvez, M. G. Alberti and A. Enfedaque, "Assessment of the shear behaviour of polyolefin fibre reinforced concrete and verification by means of digital image correlation," *Construction and Building Materials,* vol. Volume 181, pp. 565-578, 2018.

[2] M. D. Prisco, M. Lamperti, S. Lapolla and R. Khurana, "HPFRCC thin plates for precast roofing," de *Proceedings of second international symposium on ultra high performance concrete*, 2008.

[3] A. Caverzan, E. Cadoni and M. D. Prisco, "Dynamic tensile behavior of self-compacting steel fibre reinforced concrete," *Appl Mech Mater,* vol. 82, pp. 220-225, 2011.

[4] T. Lok and P. Zhao, "Impact response of steel fiber-reinforced concrete using a split Hopkinson pressure bar," *J Mater Civil Eng,* vol. 16, nº 1, pp. 4-9, 2004.

[5] fib Model Code, Model Code, Paris: Fédération Internationale du Béton fib/International Federation for Structural Concrete, 2010.

Peer-reviewed version available at Materials 2019, 12, 3656; doi:10.3390/ma12223656

[6] M. G. Alberti, A. Enfedaque, J. C. Gálvez and L. Pinillos, "Structural Cast-in-Place Application of Polyolefin Fiber–Reinforced Concrete in a Water Pipeline Supporting Elements," *Journal of Pipeline Systems Engineering and Practice,* vol. 8(4), 2017.

[7] M. G. Alberti, A. Enfedaque and J. C. Gálvez, "Improving the Reinforcement of Polyolefin Fiber Reinforced Concrete for Infrastructure Applications," *Fibers,* vol. 3(4), pp. 504-522, 2015.

[8] M. G. Alberti, A. Enfedaque and J. C. Gálvez, "On the mechanical properties and fracture behavior of polyolefin fiber-reinforced self-compacting concrete," *Construction and Building Materials,* vol. Volume 55, pp. 274-288, 2014.

[9] M. G. Alberti, A. Enfedaque, J. C. Gálvez and V. Agrawal, "Reliability of polyolefin fibre reinforced concrete beyond laboratory sizes and construction procedures," *Composite Structures,* vol. 140(15), pp. 506-524, 2016.

[10] J. Ferreira and F. Branco, "Structural application of GRC in telecommunication towers," *Constr. Build. Mater.,* vol. 21, nº 1, p. 19–28, 2007.

[11] M. Polanco-Loria, Numerical modelling of plain and reinforced concrete by damage mechanics, Trondheim : Department of Structural Engineering, Norwegian University of Science and Technology, 1997.

[12] A. Duarte, B. Silva, N. Silvestre, J. d. Brito, E. Júlio and J. Castro, "Finite element modelling of short steel tubes filled with rubberized concrete," *Composite Structures,* vol. 150, pp. 28-40, 2016.

[13] A. Duarte, N. Silvestre, J. d. Brito and E. Júlio, "Numerical study of the compressive mechanical behaviour of rubberized concrete using the eXtended Finite Element Method (XFEM)," *Composite Structures,* vol. 179, pp. 132-145, 2017.

[14] H. Pham, R. Al-Mahaidi and V. Saouma, "Modelling of CFRP–concrete bond using smeared and discrete cracks," *Composite Structures,* vol. 75, nº 1–4, pp. 145-150, 2006.

[15] Z. H. Feiyu Liao, "An extended finite element model for modelling localised fracture of reinforced concrete beams in fire," *Computers & Structures,* vol. 152, pp. 11-26, 2015.

[16] A. Hillerborg, M. Modéer and P. E. Petersson, "Analysis of crack formation and crack growth in concrete by means of fracture mechanics and finite elements," *Cement and concrete research,* vol. 6(6), pp. 773-78, 1976.

[17] E. Reyes, J. C. Gálvez, M. J. Casati, D. A. Cendón, J. M. Sancho and J. Planas, "An embedded cohesive crack model for finite element analysis of brickwork masonry fracture," *Engineering Fracture Mechanics,* vol. 76, nº 12, pp. 1930-1944, 2009.

[18] J. C. Gálvez, J. Planas, J. M. Sancho, E. Reyes, D. A. Cendón and M. J. Casati, "An embedded cohesive crack model for finite element analysis of quasi-brittle materials," *Engineering Fracture Mechanics,* vol. 109, pp. 369-386, 2013.

[19] J. M. Sancho, J. Planas, D. A. Cendón, E. Reyes and J. C. Gálvez, "An embedded crack model for finite element analysis of concrete fracture," *Engineering Fracture Mechanics,* vol. 74, nº 1, pp. 75-86, 2007.

[20] J. C. Gálvez, J. Červenka, D. Cendón and V. Saouma, "A discrete crack approach to normal/shear cracking of concrete," *Cement and Concrete Research,* vol. 32, nº 10, pp. 1567-1585, 2002.

[21] EN 12390-13, Testing hardened concrete - Part 13: Determination of secant modulus of elasticity in compression, 2013.

[22] EN 14651:2007+A1, Test method for metallic fibre concrete. Measuring the flexural tensile strength (limit of proportionality (LOP), residual), 2007.

[23] RILEM TC-162-TDF, "Bending test: Final recommendations.," 2002.

[24] EN 12390-6, "Testing hardened concrete. Part 6. Tensile spliting strength of test specimens," 2009.

[25] A. Caggiano, G. Etse and E. Martinelli, "Zero-thickness interface model formulation for failure behavior of fiber-reinforced cementitious composites," *Computers & Structures,* vol. 98, pp. 23-32, 2012.

[26] V. Slowik, B. Villmann, N. Bretschneider and T. Villmann, "Computational aspects of inverse analyses for determining softening curves of concrete," *Computer Methods in Applied Mechanics and Engineering,* vol. 195, nº 52, p. 7223–7236, 2006.

[27] S. T. Kang and J. K. Kim, "The relation between fiber orientation and tensile behavior in an Ultra High Performance Fiber Reinforced Cementitious Composites (UHPFRCC)," *Cement and Concrete Research,* vol. 41(10), pp. 1001-1014, 2011.

[28] S. T. Kang, B. Y. Lee, J. K. Kim and Y. Y. Kim, "The effect of fibre distribution characteristics on the flexural strength of steel fibre-reinforced ultra high strength concrete," *Construction and Building Materials,* vol. 25(5), pp. 2450-2457, 2011.

[29] A. Enfedaque, M. G. Alberti, J. C. Gálvez and J. Domingo, "Numerical simulation of the fracture behaviour of glass fibre reinforced cement," *Construction and Building Materials,* vol. 136, pp. 108-117, 2017.

[30] J. Planas and Z. P. Bazant, Fracture and size effect in concrete and other quasibrittle materials, CRC press, 1997.

[31] G. V. Guinea, J. Planas and M. Elices, "A general bilinear fit for the softening curve of concrete," *Materials and Structures,* vol. 27, nº 2, pp. 99-105, 1994.

[32] de Oliveira e Sousa, J. L. A. and Gettu, R., "Determining the tensile stress-crack opening curve of concrete by inverse analysis," *Journal of engineering mechanics*, 132(2), 141-148.

[33] M. G. Alberti, "Polyolefin fibre-reinforced concrete: from material behaviour to numerical and design considerations," Doctoral Thesis, Universidad Politécnica de Madrid, 2015.

[34] J. Planas, G. Guinea, J. Gálvez, B. Sanz and A. Fathy, "Indirect test for stress-crack opening curve," de *Experimental Determination of the Stress-Crack Opening Curve for Concrete in Tension - Final report of RILEM Technical Committee TC 187-SOC*, J. Planas, Ed., RILEM Publications SARL, 2007, pp. 13-29.